IPEM Institute of Physics and Engineering in Medicine

PAPER • OPEN ACCESS

Dosimetric accuracy and radiobiological implications of ion computed tomography for proton therapy treatment planning

To cite this article: Sebastian Meyer *et al* 2019 *Phys. Med. Biol.* **64** 125008

View the article online for updates and enhancements.

Recent citations

- Prediction of image noise contributions in proton computed tomography and comparison to measurements
  J Dickmann *et al*

Physics in Medicine & Biology

IPEM Institute of Physics and Engineering in Medicine

PAPER

Dosimetric accuracy and radiobiological implications of ion computed tomography for proton therapy treatment planning

Sebastian Meyer[1,10] , Florian Kamp[2], Thomas Tessonnier[3,8], Andrea Mairani[4,5], Claus Belka[2,6], David J Carlson[7,9], Chiara Gianoli[1] and Katia Parodi[1]

[1] Department of Medical Physics, Ludwig-Maximilians-Universität München, Garching b. München, Germany
[2] Department of Radiation Oncology, University Hospital, LMU Munich, Munich, Germany
[3] Department of Radiation Oncology and Radiation Therapy, Heidelberg University Hospital, Heidelberg, Germany
[4] Heidelberg Ion Beam Therapy Center, University Hospital Heidelberg, Heidelberg, Germany
[5] Fondazione CNAO, Unità di Fisica Medica, Pavia, Italy
[6] German Cancer Consortium, Munich, Germany
[7] Department of Therapeutic Radiology, Yale University School of Medicine, New Haven, CT, United States of America
[8] Current affiliation: Medical Physics Department, Centre François Baclesse, Caen, France
[9] Current affiliation: University of Pennsylvania, Department of Radiation Oncology, Philadelphia, PA, USA
[10] The author to whom correspondence may be addressed.

E-mail: Meyer.Se@physik.uni-muenchen.de

Abstract

Ion computed tomography (iCT) represents a potential replacement for x-ray CT (xCT) in ion therapy treatment planning to reduce range uncertainties, inherent in the semi-empirical conversion of xCT information into relative stopping power (RSP). In this work, we aim to quantify the increase in dosimetric accuracy associated with using proton-, helium- and carbon-CT compared to conventional xCT for clinical scenarios in proton therapy. Three cases imaged with active beam-delivery using an ideal single-particle-tracking detector were investigated using FLUKA Monte-Carlo (MC) simulations. The RSP accuracy of the iCTs was evaluated against the ground truth at similar physical dose. Next, the resulting dosimetric accuracy was investigated by using the RSP images as a patient model in proton therapy treatment planning, in comparison to common uncertainties associated with xCT. Finally, changes in relative biological effectiveness (RBE) with iCT particle type/spectrum were investigated by incorporating the repair-misrepair-fixation (RMF) model into FLUKA, to enable first insights on the associated biological imaging dose. Helium-CT provided the lowest overall RSP error, whereas carbon-CT offered the highest accuracy for bone and proton-CT for soft tissue. For a single field, the average relative proton beam-range variation was -1.00%, $+0.09\%$, -0.08% and -0.35% for xCT, proton-, helium- and carbon-CT, respectively. Using a 0.5%/0.5mm gamma-evaluation, all iCTs offered comparable accuracy with a better than 99% passing rate, compared to 83% for xCT. The RMF model predictions for RBE for cell death relative to a diagnostic xCT spectrum were 0.82–0.85, 0.85–0.89 and 0.97–1.03 for proton-, helium-, and carbon-CT, respectively. The corresponding RBE for DNA double-strand break induction was generally below one. iCT offers great clinical potential for proton therapy treatment planning by providing superior dose calculation accuracy as well as lower physical and potentially biological dose exposure compared to xCT. For the investigated dose level and ideal detector, proton-CT and helium-CT yielded the best performance.

1. Introduction

Ion computed tomography (iCT) represents a promising solution for direct assessment of the relative (to water) ion stopping power (RSP). Thereby, uncertainties of 1%–3% inherent in the semi-empirical conversion of x-ray CT (xCT) Hounsfield units (HU) into RSP (Paganetti 2012, Yang *et al* 2012) could be eliminated. This would allow

for a reduction of the related safety margins for improving the clinical outcome of patients receiving ion therapy treatments. In order to potentially replace x-ray imaging for proton therapy treatment planning, iCT must provide competitive image quality and dose calculation accuracy without enhancing the imaging dose exposure. This would open new perspectives for adaptive ion therapy with on-isocenter low dose imaging (Landry and Hua 2018). While dual-energy CT demonstrates already clinically promising results (Wohlfahrt *et al* 2017) in terms of reduced range uncertainties, iCT is the intuitive solution providing better RSP accuracy (Hansen *et al* 2015) with the possibility of imaging directly at the beam isocenter. Furthermore, iCT image quality is not affected by metal artifacts (Oancea *et al* 2018). Various groups worldwide are currently investigating ion imaging with a dedicated focus on proton beams (Johnson 2018). In contrast, heavier ions can yield improved image quality by benefiting from reduced multiple Coulomb scattering (MCS) (Hansen *et al* 2014, Volz *et al* 2017). However, they also exhibit an increased physical dose per particle and suffer from an elevated loss of primaries due to fragmentation, ultimately affecting the noise of iCT (Gehrke *et al* 2018). A comparison of different particle types for iCT, including image quality and range accuracy for proton therapy treatment planning in realistic clinical scenarios, remains unstudied. Additionally, a detailed assessment of the biological impact of typical iCT acquisitions is required, since ion beams can have elevated linear energy transfer (LET) spectra compared to sparsely ionizing x-rays. In this study, we addressed the image quality of proton- (pCT), helium- (heCT) and carbon-CT (cCT) in clinical scenarios using a dedicated, experimentally validated Monte-Carlo (MC) simulation framework (Meyer *et al* 2017). The associated dose calculation accuracy was quantified using the RayStation treatment planning system. Furthermore, an approach for coupling the MC-code to the mechanistic repair-misrepair-fixation (RMF) model (Carlson *et al* 2008) was implemented to derive the relative biological effectiveness (RBE) for the iCT simulations. The different scenarios were compared to the established practice using xCT both in terms of RSP uncertainties and imaging dose.

2. Materials and methods

2.1. iCT simulation and reconstruction

Current iCT prototypes are optimized for imaging of the human head (Bashkirov *et al* 2016), due to presently available maximum beam energies and the required small field of view. Furthermore, the heterogeneities and large variation of RSP from air cavities to bony structures represent a challenging anatomy that requires accurate imaging for treatment planning.

Hence, three representative cranial patient cases with clinical xCTs were investigated: a left frontobasal anaplastic astrocytoma (Pat1), a nasopharynx cancer (Pat2) and a left sided glioblastoma (Pat3). The iCT simulations were performed using the FLUKA MC-code (Ferrari *et al* 2005, Böhlen *et al* 2014) (version 2011.2c.6 using HADROTHE defaults without explicit δ-ray production) with customized user routines in order to mimic a realistic scanned beam with an experimentally validated beam model (Tessonnier *et al* 2016). In this work, we simulated an ideal detector represented by two scoring planes recording position, direction and energy of each individual ion. These trackers each covered an area of 30×30 cm^2 and are located prior and posterior to the imaged patient volume, 45 cm from the isocenter as in a realistic clinical scenario. The initial energy was set to the nominal beam energy E222 of the Heidelberg Ion-Beam Therapy Center, which corresponds to a range in water of ~26 cm for each of the ions, being hypothetically detectable with existing prototype detector systems (Giacometti *et al* 2017). A total of 400 protons, 100 helium ions or 20 carbon ions were simulated per irradiation spot for 180 projections, resulting in a ~1.9 mGy physical dose for each case, which is much lower than typical values between 10 mGy and 100 mGy in xCT (Murphy *et al* 2007). The spot spacing was chosen in accordance with the resolution of the patient xCT data, i.e. 1.074 mm and 3 mm in the horizontal and vertical direction, respectively. The xCTs in DICOM format were imported in FLUKA and converted to the RSP ground truth by forcing the MC-code to follow a bijective and error-free clinical-like HU-RSP conversion curve (Parodi *et al* 2007). In contrast to a real patient scenario, the HU-RSP curve employed in an MC simulation does not contain any uncertainty, since it is defined by the user and is in this work monotonic and bijective. Based on the knowledge of the conversion curve, the patient's xCT anatomy is converted into RSP without uncertainty, thus defining the ground truth reference map. Hence, the exact RSP distribution of the simulated patient anatomy in FLUKA is known. The only remaining uncertainty in the presented approach originates from the energy dependency of RSP which is negligible for the used energies (Arbor *et al* 2015).

For tomographic image reconstruction of the iCTs, the iterative ordered-subset simultaneous algebraic reconstruction technique (Wang and Jiang 2004) with incorporated cubic spline path (CSP) estimate (Collins-Fekete *et al* 2015) and total variation superiorization was implemented. Furthermore, the common 3σ data cuts (Schulte *et al* 2008) were used for the retrieved events. To account for the patient's surrounding air gap, a hull contour derived from the xCT data was used (Collins-Fekete *et al* 2017a). The reconstruction was stopped if

the derivative (with respect to the iteration number) of the average Euclidean data divergence was either below $2 \cdot 10^{-6}$ (cCT), $1 \cdot 10^{-7}$ (heCT) and $1 \cdot 10^{-8}$ (pCT)[11], or after 30 iteration cycles through all particle histories were completed.

The overall image quality for a reconstructed slice was assessed with respect to the known ground truth using the RSP relative error ϵ (Penfold *et al* 2010) defined as

$$\epsilon = \frac{\sum_i |\overline{x}_i - x_i|}{\sum_i \overline{x}_i},$$

where x_i and $\overline{x}_i$ are the RSP values in voxel i of the reconstructed and ground truth image (obtained from the patient anatomy of the xCT and the HU-RSP conversion of the MC simulation), respectively. The joint histogram of the reconstructed iCT and the original HU values in the corresponding ground truth enabled the calculation of the RSP precision as a measure of noise of the iCT images.

2.2. FLUKA-RMF coupling for RBE prediction

In the RMF model, developed by Carlson *et al* (2008), double-strand break (DSB) induction and processing are explicitly linked with reproductive cell death. For a given particle radiation, the terms of the linear-quadratic (LQ) model can be derived from the formalisms presented in Frese *et al* (2012) and Kamp *et al* (2015) using the tissue-specific LQ radiosensitivity parameters (α_X and β_X), the initial number of induced DSBs (Σ) and the frequency-mean specific energy ($\overline{z}_F$) for the reference radiation and the considered radiation.

MC damage simulation (MCDS) (Semenenko and Stewart 2004, Stewart *et al* 2011) (version 3.10A with default settings) was used to predict Σ and $\overline{z}_F$ as a function of particle type and energy under normoxic conditions. The corresponding parameters for the reference radiation were obtained by simulating the secondary electron energy spectrum of a ^{60}Co source (Hsiao and Stewart 2008) ($\Sigma_X = 8.2706\,\mathrm{Gbp}^{-1}\,\mathrm{Gy}^{-1}, \overline{z}_{F,X} = 0.0019\,\mathrm{Gy}$).

In order to account for the RBE of different ion types and energy spectra, the RMF-derived predictions of the LQ parameters were coupled to the FLUKA MC-code following the approach of Mairani *et al* (2010). In each voxel, the RBE for cell death ($\mathrm{RBE_{RMF}}$) can be calculated from the dose-weighted average LQ radiosensitivity parameters and the RBE for DSB induction ($\mathrm{RBE_{DSB}}$) can be computed using MCDS. For performing an online adaption of the tissue-specific radiosensitivity parameters within the framework of the RMF model, we adapted the approach of Kamp *et al* (2017). In a similar manner, the reference radiation quality (i.e. Σ_X and $\overline{z}_{F,X}$) can be changed. This feature was exploited to calculate the biological dose response for a diagnostic 130 kVp x-ray energy spectrum obtained for a tungsten anode with 0.8 mm beryllium filtration (Stewart *et al* 2015) ($\Sigma_X = 10.4749\,\mathrm{Gbp}^{-1}\,\mathrm{Gy}^{-1}, \overline{z}_{F,X} = 0.0392\,\mathrm{Gy}$[12]) as reference imaging radiation. This previously investigated setting can serve as the best-case scenario for xCT, yielding slightly reduced biological effects in comparison to the more typically chosen tube voltage of 120 kVp for x-ray imaging treatment planning.

2.3. Treatment planning and dose calculation

For each case, proton therapy treatment plans using pencil beam scanning were optimized on the RSP ground truth obtained from the imported xCT anatomy. A research version of the commercial treatment planning system RayStation (RaySearch Laboratories, Sweden) was used for all dose calculations of the treatment planning comparison within this work. The derived treatment plans were recalculated in RayStation using the simulated iCTs. Since RayStation does not currently support direct RSP import, the reconstructed RSP images were converted into HUs using the inverse of the HU-RSP conversion curve of the MC-code, relying on the imposed bijectivity of that function. Subsequently, all images were imported in the treatment planning system using the same internal conversion to density and RSP, eliminating possible uncertainties related to the image import. This procedure allows a consistent comparison independent of the fact that the conversion exploited in the MC simulation is different from the one of the TPS. In order to emulate the typical uncertainties encountered for the HU-RSP conversion using conventional xCT, we additionally imported the xCTs by randomly introducing an error (using a continuous distribution from -3% to 3%) to the RSP values of the conversion curve. We chose a curve that systematically overestimates the RSP for soft tissue while underestimating it for bone, in agreement with findings of Wohlfahrt *et al* (2017).

The obtained results were compared to the original (planned) dose distributions by means of beam's-eye view range difference maps for single field uniform doses, dose-volume histograms and global 3D gamma evaluation (Podesta *et al* 2014) (using a 10% low-dose threshold) for multi-field intensity modulated proton therapy plans. The single field plans were chosen in a way to represent cases of large heterogeneities (Pat1) as well as more homogeneous beam paths with long (Pat2) and short penetration depth (Pat3). The obtained range differences were converted into a water-equivalent range by performing a raytracing between the 80% distal dose points and

---

[11] The chosen values yield the best compromise between convergence and noise for the different particle statistics.

[12] $\overline{z}_{F,X}$ for a spherical water target was approximated by $\overline{z}_{F,X} = 0.204 \frac{\mathrm{LET}}{d_{tar}^2} \left(\frac{\mathrm{keV}}{\mu\mathrm{m}^3} \right)$ with $d_{tar} = 5\,\mu\mathrm{m}$ (Carlson *et al* 2008).

weighting the intersected voxels with the RSP of the ground truth (Wohlfahrt *et al* 2017). To obtain relative range shifts, the values were divided by the corresponding water-equivalent range for the reference scenario.

3. Results

3.1. Evaluation of iCT image quality

Figure 1 shows axial slices of the reconstructed iCTs and the related RSP relative errors. In general, heCT exhibits superior image quality in terms of reduced RSP error, being on average 0.2% and 0.3% lower than for pCT and cCT, respectively. For heterogeneous regions like the paranasal sinuses or nasal cavities (e.g. slice 28–35 in figure 1(J)), an increased relative error becomes evident. In regions mainly containing homogeneous brain tissue, (e.g. slice 42–47 in figure 1(J)), the pCT image quality exceeds that of the cCT and yields RSP relative errors comparable to the heCT. When using the same statistics for pCT and heCT as for cCT, the average RSP relative error over all reconstructed slices was 6.6%, 1.7% and 1.3% for pCT, heCT and cCT, respectively.

Figure 2 displays the obtained RSP distribution for Pat3, demonstrating good agreement with the ground truth HU-RSP conversion curve. pCT and cCT show worse RSP precision in terms of an increased standard deviation, being 1.3 times higher than for heCT. In the zoom-in plots of figure 2, the reconstructed RSP is underestimated for bony materials (-2.1%, -1.2% and -0.4% at 1500 HU for pCT, heCT and cCT, respectively) and overestimated for fat and soft tissue ($+0.5\%$, $+0.9\%$ and $+1.2\%$ at 0 HU).

3.2. Assessment of range accuracy

For single field uniform dose proton therapy plans, figure 3 shows the observed range variations, calculated as water-equivalent differences in the position of the 80% distal dose falloff in beam's-eye view between planned (ground truth) and recalculated (iCTs and xCT) dose distribution. All iCT cases show sub-millimeter accuracy with an average (± 1 s.d.) relative proton-beam range error of $(+0.09 \pm 0.33)\%$, $(-0.08 \pm 0.24)\%$ and $(-0.35 \pm 0.26)\%$ for pCT, heCT and cCT, respectively. This corresponds to a water-equivalent range error of $(+0.07 \pm 0.18)$ mm, (-0.08 ± 0.14) mm and (-0.29 ± 0.18) mm. For the pCT data set of Pat2, over-ranging above 1.0% was observed for pencil beams traversing the nasal cavities. The range error for xCT was $(-1.00 \pm 0.43)\%$ and (-0.84 ± 0.32) mm.

3.3. Comparison of dosimetric outcome

The dosimetric comparison based on clinical multi-field intensity modulated proton therapy plans is presented in figure 4. The obtained iCT dose-volume histograms were in notable agreement with the reference and variations in $D_{2\%}$ and $D_{98\%}$ were not exceeding 15 cGy for organs at risk. By contrast, variations of up to 200 cGy were observed for xCT. For a 0.5%/0.5mm gamma-evaluation, xCT exhibited an average passing rate of 83% increasing to better than 99% for all iCTs.

3.4. Estimation of biological dose exposure

Table 1 lists the mean RBE predictions for the three iCT simulation scenarios for the biological endpoints of DSB induction and cell death. RBE_{DSB} was 1.4%, 1.8% and 2.3% lower than RBE_{RMF} assuming an α/β of 10 Gy for pCT, heCT and cCT, respectively. The corresponding unrestricted dose-averaged LET values (in water) (Bauer *et al* 2014) were 2.33 keV μm^{-1}, 4.00 keV μm^{-1} and 11.85 keV μm^{-1}. On average (including all presented biological modeling), the RBE for pCT was 3.8% lower than for heCT and 18.9% lower than for cCT.

4. Discussion

In the presented study, we demonstrated that iCT can provide accurate RSP images which allow treatment planning with small range uncertainties and very good dosimetric accuracy at a low physical and biological dose exposure.

4.1. Evaluation of iCT image quality

While all iCTs provided accurate RSP values (figure 1), differences mainly arise from variations in the path estimation accuracy and the number of particles at the investigated dose. Despite the most accurate path estimate, reduced statistics due to fragmentation and high stopping power cause an increased noise for cCT (figure 1(H)). The implemented CSP offers similar accuracy as the computationally more demanding most likely path and is superior to a straight path even for cCT, despite the substantially reduced MCS (Collins-Fekete *et al* 2017a).

The use of a hull contour for the CSP estimation is of fundamental importance (Collins-Fekete *et al* 2017b). Although the selected approach exploited prior knowledge, an approximated image reconstructed along straight trajectories (Shrestha *et al* 2018) or geometrically (Giacometti *et al* 2017) could be alternatively used.
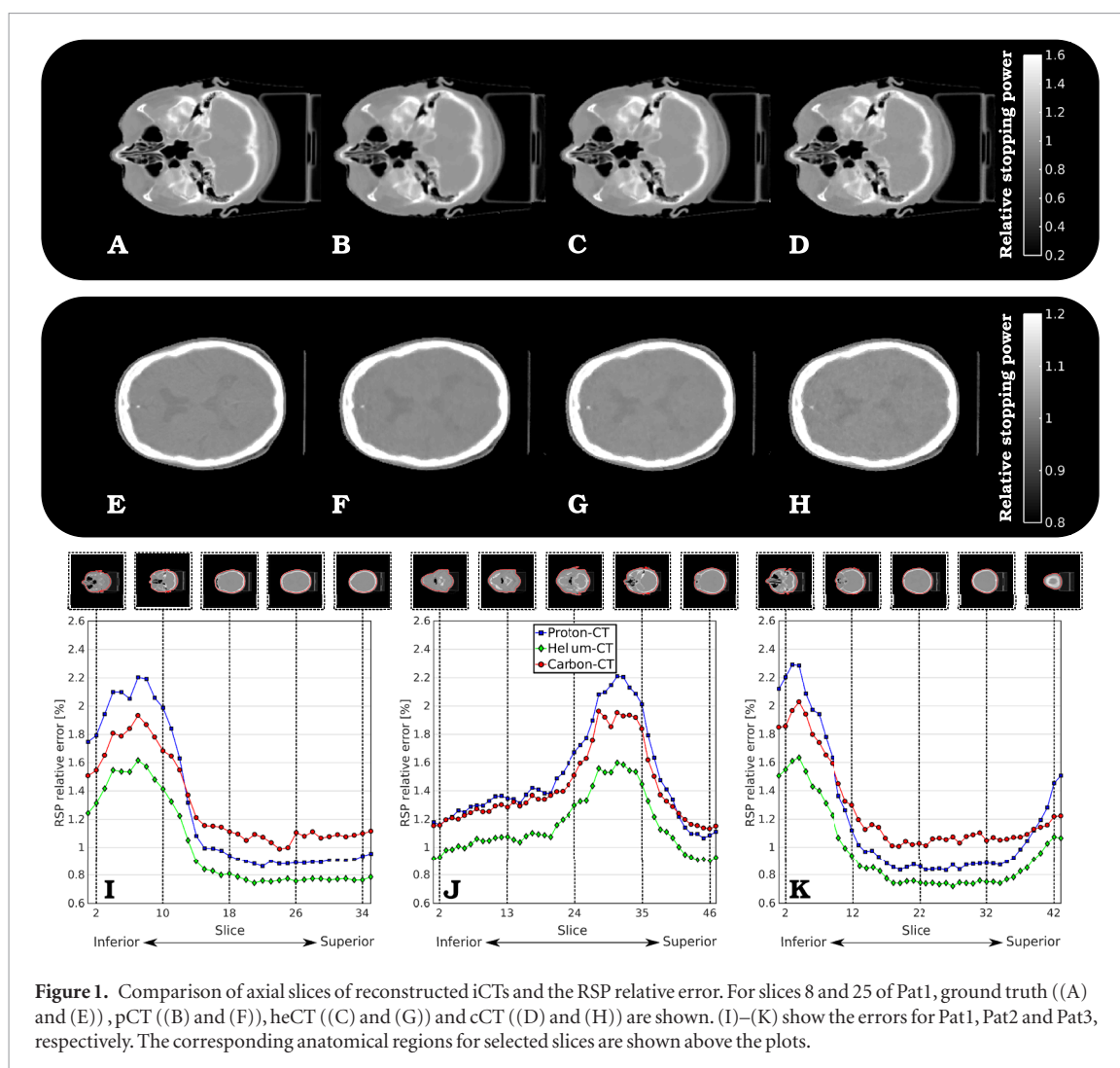
Figure 1. Comparison of axial slices of reconstructed iCTs and the RSP relative error. For slices 8 and 25 of Pat1, ground truth ((A) and (E)), pCT ((B) and (F)), heCT ((C) and (G)) and cCT ((D) and (H)) are shown. (I)–(K) show the errors for Pat1, Pat2 and Pat3, respectively. The corresponding anatomical regions for selected slices are shown above the plots.

The increased RSP relative error for heterogeneities (figure 1(J), slice 28–35) originates from the reduced RSP accuracy for bone and low-HU regions (figure 2) caused by partial volume effects and path estimation inaccuracies. The latter is related to the assumption of homogenous water in the CSP model (Collins-Fekete *et al* 2015). Both effects are enhanced for pCT due to increased scattering. In contrast, for soft tissue, the path estimations are comparably accurate for all ions. Here, pCT provides superior accuracy due to less noise from an increased number of particles at the same imaging dose. This is supported by the large RSP error of pCT compared to heCT and cCT observed at the same particle statistics. The remaining RSP inaccuracy (figure 2) introduced by the reconstruction demonstrates the current limitation of iCT even for an ideal setup.

4.2. Assessment of range accuracy

Figure 3 illustrates the influence of RSP errors on the dose calculation accuracy in different anatomical regions. Overall, heCT showed superior performance since it is less affected by heterogeneities than pCT and offers high RSP accuracy for soft tissue (figure 2), representing the main penetration medium. The achieved range accuracy of better than 0.4% surpasses the uncertainty of xCT being typically 1%–3% (Yang *et al* 2012) and −1.00% in the presented case. The xCT range shift is comparable to those found by Wohlfahrt *et al* (2017) for a comparison with dual-energy CT based RSP estimation, reporting average shifts significantly larger than 1%. A negative sign (i.e. range underestimation) is expected since the beam mainly penetrates soft tissue, which has systematically larger RSP than the reference. This demonstrates that iCT could potentially provide reduced range uncertainties for proton therapy treatment planning for the considered anatomical locations compared to xCT. However, experimental realizations are not yet addressed by this theoretical study. Potentially reduced gain in treatment plan quality is expected due to the degraded image quality for a realistic detector system. The RSP accuracy is mainly influenced by the water-equivalent path length (WEPL) resolution of the residual range/energy detector. However, if the WEPL resolution is close to the intrinsic range straggling limit, e.g. around 3 mm for 200 MeV protons (Bashkirov *et al* 2016), the MC simulations implicitly embed this uncertainty and therefore its impact on RSP accuracy. The spatial resolution is limited by the ion track estimation accuracy which depends on the
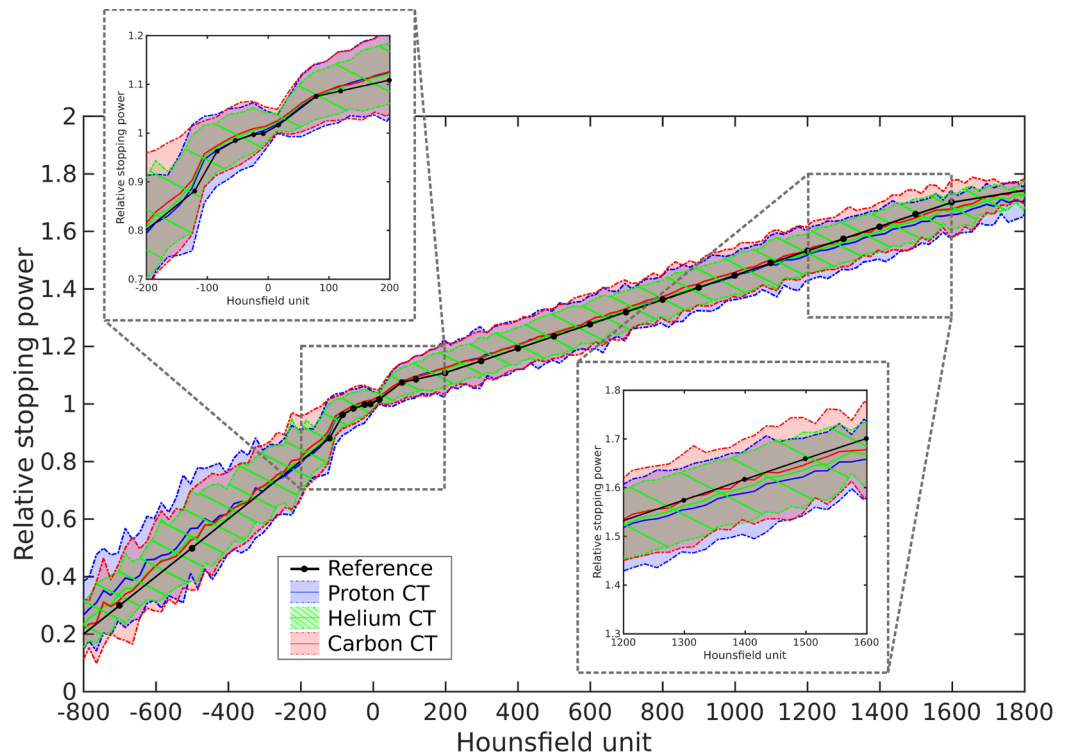
Figure 2. Joint histogram of the reconstructed iCTs and the original HU values, shown in steps of 20 HU values. The colored solid lines correspond to the mean value while partially-transparent shaded areas represent the ± 3 standard deviation interval. An outline is added to improve the visibility of overlapping regions. The black line indicates the ground truth conversion curve being used to import the initial xCT into the simulation.
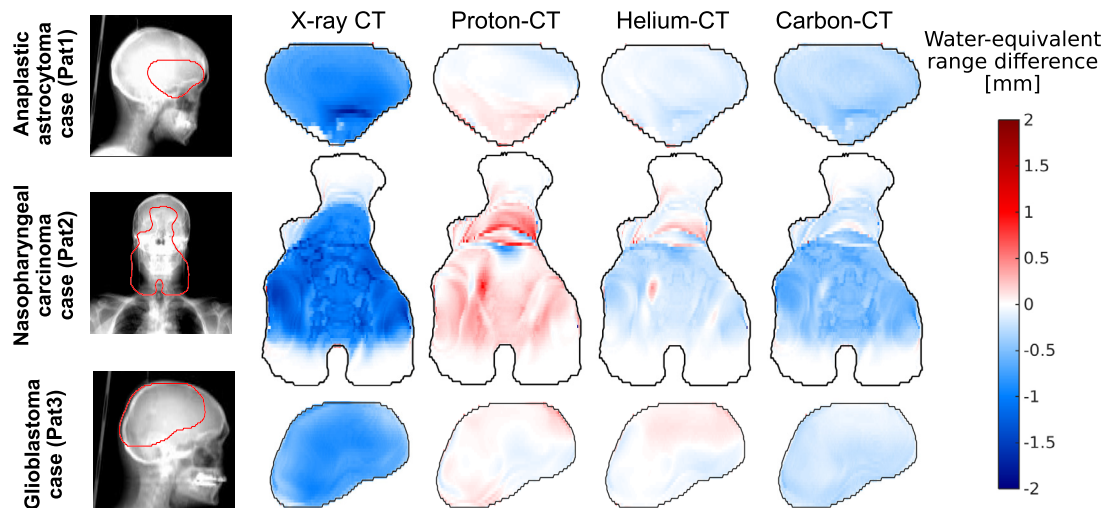

Figure 3. Beam's-eye view water-equivalent proton range variations for recalculation based on iCTs and xCT with respect to the optimized dose using the reference plan. On the left, the 80% isodose contours are overlaid with the ground truth radiographies. Positive and negative differences indicate an over- and under-ranging, respectively.

location and properties of the tracking detectors, and the intrinsic inaccuracy of the employed path model. While the latter is included in our study, spatial resolution and material budget of typical pCT prototypes will cause an average position uncertainty of 0.7 mm (Bopp *et al* 2014). Heavier particles will benefit from reduced scattering in the innermost tracker halves, being a further argument in favor of helium ions compared to protons. Additionally, fragmentation within the detector material will further degrade the available particle statistics, thus increasing the necessary imaging dose in order to safeguard the same image quality.

The general range underestimation is related to an average RSP overestimation, which in turn might have two potential underlying causes. First, the conversion of the energy loss of each individual ion into integrated RSP is based on the Bethe-Bloch formula, neglecting energy loss due to other interaction types (e.g. nuclear reactions).
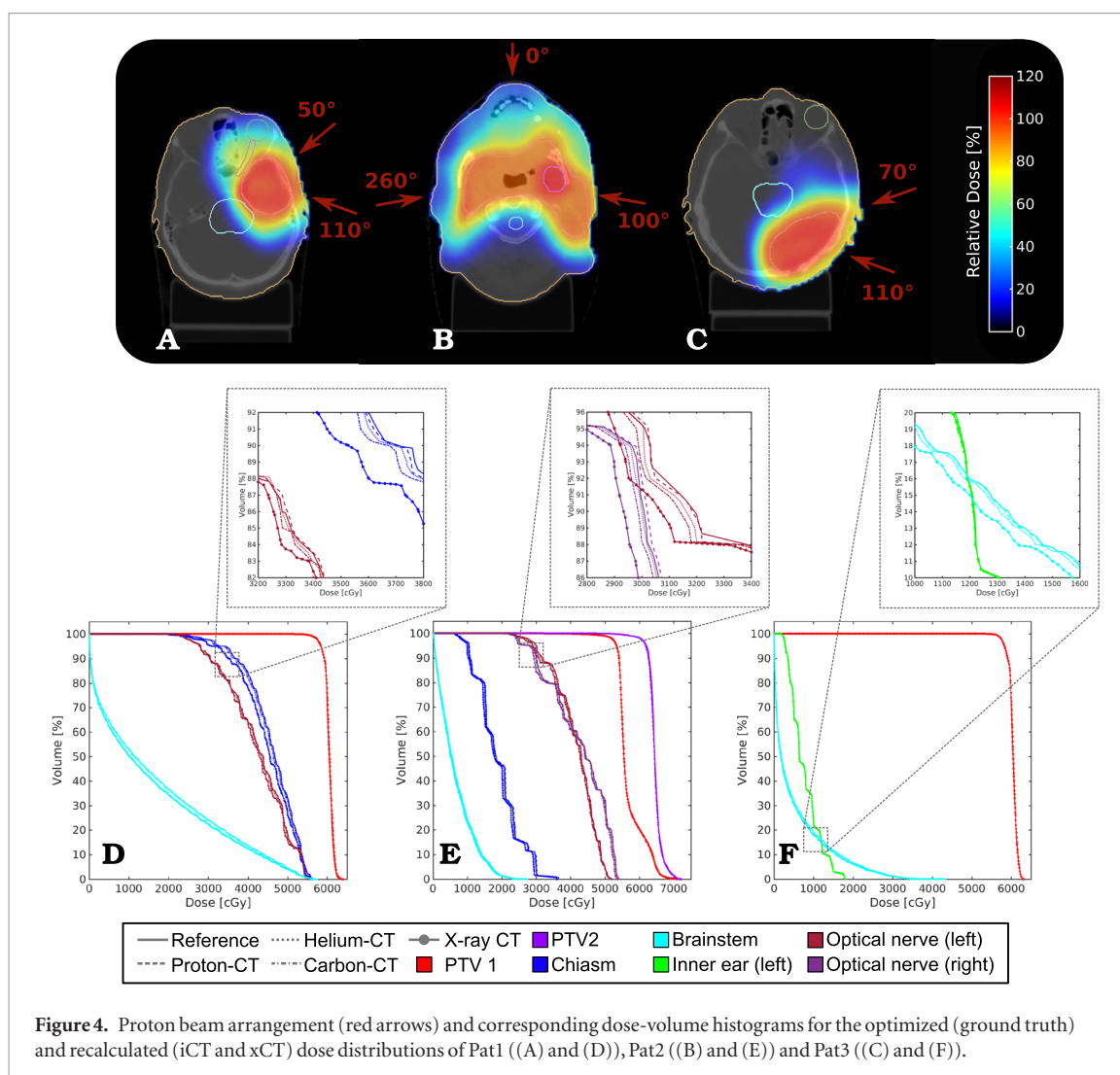
Figure 4. Proton beam arrangement (red arrows) and corresponding dose-volume histograms for the optimized (ground truth) and recalculated (iCT and xCT) dose distributions of Pat1 ((A) and (D)), Pat2 ((B) and (E)) and Pat3 ((C) and (F)).

However, the resulting overestimation effect is small, since the applied data cuts (Schulte *et al* 2008) should have removed the majority of events with nuclear collisions and large-angle MCS. Secondly, the fit factors of the CSP model have some uncertainty and simply assume uniform homogenous material (Collins-Fekete *et al* 2015). Therefore, the scattering and consequently the path segment length in bone is underestimated, causing an RSP overestimation (neglecting partial volume effects). Generally, the RSP overestimation for very small HU values seems to be mostly compensated by the underestimation for bone regions.

4.3. Comparison of dosimetric outcome

Figure 4 compares the impact of range calculation uncertainties on the dose distribution for clinical proton therapy plans. The very promising dosimetric outcome is confirmed by high gamma passing-rates, which are in agreement with the observed range accuracy (figure 3). Variations between the different ions were not substantial due to similar RSP accuracies (figure 1) and relatively robust treatment plans.

This demonstrates the potential of iCT as a replacement for x-ray imaging. However, various clinical studies have already shown that recent developments in x-ray imaging technology like dual-energy CT can also provide improved treatment planning accuracy (Wohlfahrt *et al* 2017). While those devices already exist as clinical products, they are typically not integrated at isocenter and the RSP accuracy should still be theoretically inferior to iCT (Hansen *et al* 2015).

Integrating iCT into clinical practice will require a dedicated and adjusted work-flow. Even though iCT enables improved density resolution (Schulte *et al* 2005), the contrast might be insufficient for accurate tumor detection and delineation. High-density contrast agents like gold nanoparticles (Hainfeld *et al* 2006) could in principle provide sufficient contrast enhancement if the cellular intake is appropriate (Schulte *et al* 2004). iCT will potentially allow us to perform treatment delivery and planning inside the treatment room without requiring repositioning of the patient or additional imaging technology. This will avoid further range uncertainties if fast solutions for image reconstruction (e.g. GPU implementations (Karonis *et al* 2013)), as well as delineation and treatment planning, are available.

Table 1. Estimated mean RBE in the total imaging volume of the iCT simulations. RBE_{RMF} is the RBE for cell death predicted by the RMF model for assumed reference tissue radiosensitivity of $\alpha/\beta = 2$ Gy and $\alpha/\beta = 10$ Gy. RBE_{DSB} is the RBE for DNA double-strand break induction using the MCDS algorithm.

	Proton-CT			Helium-CT			Carbon-CT		
Patient	$RBE_{RMF}^{2\,Gy}$	$RBE_{RMF}^{10\,Gy}$	RBE_{DSB}	$RBE_{RMF}^{2\,Gy}$	$RBE_{RMF}^{10\,Gy}$	RBE_{DSB}	$RBE_{RMF}^{2\,Gy}$	$RBE_{RMF}^{10\,Gy}$	RBE_{DSB}
Reference radiation: ^{60}Co									
Pat1	1.138	1.055	1.034	1.192	1.089	1.064	1.381	1.240	1.205
Pat2	1.126	1.051	1.032	1.188	1.090	1.065	1.386	1.243	1.208
Pat3	1.126	1.052	1.032	1.182	1.087	1.063	1.379	1.240	1.205
Reference radiation: 130 kVp									
Pat1	0.850	0.823	0.816	0.888	0.849	0.840	1.026	0.966	0.951
Pat2	0.843	0.821	0.815	0.886	0.850	0.841	1.029	0.969	0.954
Pat3	0.843	0.821	0.815	0.882	0.848	0.839	1.024	0.966	0.952

4.4. Estimation of biological dose exposure

Table 1 summarizes the RMF model predictions of the RBE for cell death for the different iCT simulations. The use of a diagnostic x-ray imaging spectrum as reference radiation allows us to evaluate radiobiological implications encountered when using iCT as a replacement of xCT for treatment planning imaging. The considerable changes in RBE_{DSB} with reference radiation are in agreement with a previously reported value of 1.259 for the RBE_{DSB} of 130 kVp x-rays relative to ^{60}Co γ-rays (Stewart *et al* 2015). In general, all RBE_{DSB} values relative to the 130 kVp x-ray spectrum were below 1, indicating reduced radiobiological implications compared to x-ray imaging, since the patient is solely receiving dose from the low-LET region of the Bragg-curve plateau. The processing of DSBs into chromosome aberrations is widely considered a dominant mechanism for reproductive cell death and radiation induced carcinogenesis (Byrne *et al* 2014). We consider the latter of great importance and as a major biological endpoint for imaging applications.

In addition, RBE_{RMF} directly provides an estimate of the RBE for reproductive cell death based on the LQ model. While this formalism is well established at treatment doses, an underestimation of the radiation effects, the so-called low-dose hyper-radiosensitivity (Marples and Collis 2008), may occur below 1 Gy. Therefore, there is some uncertainty in the LQ/RMF RBE estimates under the investigated conditions. In addition, we are not attempting to estimate absolute survival, rather a relative measure of biological effectiveness between different particles at the same dose level.

The used RMF model estimations implicitly included δ-rays since the MCDS is tuned to experimental data and track structure simulations. Accordingly, the MC simulations used a continuous-slowing-down-approximation. For clinical energies, this approach results in dose variations below 0.7% compared to the explicit tracking of delta electrons (Mairani *et al* 2010). Despite the range of secondary electrons up to several millimeters in the iCT energy regime, the dose discrepancy is still small, with maximum variations of 0.2 mGy for cCT.

The sparse availability of data on biological effects for typical imaging doses imposes an important limitation for the presented study. However, experimental data used for validating the MCDS algorithm indicate that the number of γ-H2AX foci is linearly correlated with DSB induction for a dose range of approximately 1 mGy up to 2 Gy (Rothkamm and Löbrich 2003, Stewart *et al* 2011). While measurements have not necessarily been performed for every ion type over these dose ranges, there is strong experimental and theoretical evidence that DNA damage is a linear function of absorbed dose from ~1 mGy to 1000 Gy for all types of ions and energies. The cell survival at typical imaging doses might be affected by low-dose hyper-radiosensitivity observed for low- and high-LET radiation (Marples and Collis 2008). However, in this study our particular interest is in relative biological effects, rather than absolute. The relative yield of damage (RBE_{DSB}) is less sensitive to factors such as low-dose hyper-radiosensitivity, cell proliferation, cycle effects or measurement artifacts. Furthermore, it is the relative DSB yield that plays a significant role in the RMF model rather than the absolute number of DSBs per cell.

In the absence of experimental or clinical data, theoretical models represent a guidance in investigating the radiation biology of low-dose imaging. The presented simulation study represents a first theoretical step in evaluating the biological effects of iCT imaging, whereas future clinical applications for human patients will require a careful experimental validation of potential biological effects. The RMF model in combination with MCDS has been previously compared to experimental data and other clinically established models for various ion types (Semenenko and Stewart 2006, Carlson *et al* 2008, Stewart *et al* 2011, Frese *et al* 2012, Kamp *et al* 2015, Mairani *et al* 2016, Stewart *et al* 2018). The RMF model facilitates an online adaption of the biological modeling (Kamp *et al* 2017) without repeating the physical dose calculation, i.e. the computationally expensive MC simulations. Additionally, the RMF/MCDS approach provides information about both cell survival and DNA damage induction. This allows for the investigation of different biological endpoints, reference radiation qualities and tissue

radiosensitivity parameter combinations in order to estimate the range of variations of expected complications, considering the potential limitations of the radiobiological model at the given dose.

5. Conclusion

Our study quantitatively demonstrated that under ideal conditions iCT can enable an accurate assessment of clinical RSP values, showing the highest accuracy for heCT. In addition, the associated treatment planning comparison demonstrates improvements in dosimetric accuracy and range accuracy superior to uncertainties caused by the HU-RSP conversion for xCT. This would allow for reduced safety margins, ultimately limiting normal tissue damage and improving dose conformality for patient treatments. The RBE predictions using the RMF model indicated that iCT has reduced radiobiological effects compared to typical xCT spectra for treatment planning. Therefore, with proper detector development enabling to achieve results close to the presented intrinsic capabilities, iCT has the potential to replace x-ray imaging for ion-beam therapy treatment planning.

ORCID iDs

Sebastian Meyer ● https://orcid.org/0000-0002-2510-7045

References

Arbor N *et al* 2015 Monte Carlo comparison of x-ray and proton CT for range calculations of proton therapy beams *Phys. Med. Biol.* **60** 7585–99

Bashkirov V A *et al* 2016 Novel scintillation detector design and performance for proton radiography and computed tomography *Med. Phys.* **43** 664–74

Bauer J *et al* 2014 Integration and evaluation of automated Monte Carlo simulations in the clinical practice of scanned proton and carbon ion beam therapy *Phys. Med. Biol.* **59** 4635

Böhlen T *et al* 2014 The FLUKA code: developments and challenges for high energy and medical applications *Nucl. Data Sheets* **120** 211–4

Bopp C, Rescigno R, Rousseau M and Brasse D 2014 The impact of tracking system properties on the most likely path estimation in proton CT *Phys. Med. Biol.* **59** N197

Byrne M *et al* 2014 Mechanisms of oncogenic chromosomal translocations *Ann. New York Acad. Sci.* **1310** 89–97

Carlson D J, Stewart R D, Semenenko V A and Sandison G A 2008 Combined use of Monte Carlo DNA damage simulations and deterministic repair models to examine putative mechanisms of cell killing *Radiat. Res.* **169** 447–59

Collins-Fekete C-A *et al* 2015 Developing a phenomenological model of the proton trajectory within a heterogeneous medium required for proton imaging *Phys. Med. Biol.* **60** 5071

Collins-Fekete C-A *et al* 2017a A theoretical framework to predict the most likely ion path in particle imaging *Phys. Med. Biol.* **62** 1777

Collins-Fekete C-A *et al* 2017b Extension of the Fermi–Eyges most-likely path in heterogeneous medium with prior knowledge information *Phys. Med. Biol.* **62** 9207

Ferrari A, Sala P, Fassò A and Ranft J 2005 FLUKA: a Multi-Particle Transport Code *CERN Yellow Report* CERN-2005-010 ; INFN-TC-2005-11 ; SLAC-R-773 (CERN) (https://doi.org/10.5170/CERN-2005-010)

Frese M C, Yu V K, Stewart R D and Carlson D J 2012 A mechanism-based approach to predict the relative biological effectiveness of protons and carbon ions in radiation therapy *Int. J. Radiat. Oncol. Biol. Phys.* **83** 442–50

Gehrke T, Amato C, Berke S and Martišíková M 2018 Theoretical and experimental comparison of proton and helium-beam radiography using silicon pixel detectors *Phys. Med. Biol.* **63** 035037

Giacometti V *et al* 2017 Software platform for simulation of a prototype proton CT scanner *Med. Phys.* **44** 1002–16

Hainfeld J F, Slatkin D N, Focella T M and Smilowitz H M 2006 Gold nanoparticles: a new x-ray contrast agent *Br. J. Radiol.* **79** 248–53

Hansen D C *et al* 2015 A simulation study on proton computed tomography (CT) stopping power accuracy using dual energy CT scans as benchmark *Acta Oncol.* **54** 1638–42

Hansen D C, Bassler N, Sørensen T S and Seco J 2014 The image quality of ion computed tomography at clinical imaging dose levels *Med. Phys.* **41** 111908

Hsiao Y and Stewart R D 2008 Monte Carlo simulation of DNA damage induction by x-rays and selected radioisotopes *Phys. Med. Biol.* **53** 233–44

Johnson R P 2018 Review of medical radiography and tomography with proton beams *Rep. Prog. Phys.* **81** 016701

Kamp F *et al* 2015 Fast biological modeling for voxel-based heavy ion treatment planning using the mechanistic repair-misrepair-fixation model and nuclear fragment spectra *Int. J. Radiat. Oncol. Biol. Phys.* **93** 557–68

Kamp F, Carlson D J and Wilkens J J 2017 Rapid implementation of the repair-misrepair-fixation (RMF) model facilitating online adaption of radiosensitivity parameters in ion therapy *Phys. Med. Biol.* **62** N285

Karonis N T *et al* 2013 Distributed and hardware accelerated computing for clinical medical imaging using proton computed tomography (pCT) *J. Parallel Distrib. Comput.* **73** 1605–12

Landry G and Hua C-H 2018 Current state and future applications of radiological image guidance for particle therapy *Med. Phys.* **45** e1086–95

Mairani A *et al* 2010 The FLUKA Monte Carlo code coupled with the local effect model for biological calculations in carbon ion therapy *Phys. Med. Biol.* **55** 4273–89

Mairani A *et al* 2016 Biologically optimized helium ion plans: calculation approach and its *in vitro* validation *Phys. Med. Biol.* **61** 4283

Marples B and Collis S J 2008 Low-dose hyper-radiosensitivity: past, present, and future *Int. J. Radiat. Oncol. Biol. Phys.* **70** 1310–8

Meyer S *et al* 2017 Comparative Monte Carlo study on the performance of integration- and list-mode detector configurations for carbon ion computed tomography *Phys. Med. Biol.* **62** 1096

Murphy M J *et al* 2007 The management of imaging dose during image-guided radiotherapy: report of the AAPM Task Group 75 *Med. Phys.* **34** 4041–63

Oancea C *et al* 2018 PO-0888: Comparison of x-ray CT and proton based CT planning in the presence of titanium dental implants *Radiother. Oncol.* **127** S470–1

Paganetti H 2012 Range uncertainties in proton therapy and the role of Monte Carlo simulations *Phys. Med. Biol.* **57** R99

Parodi K, Ferrari A, Sommerer F and Paganetti H 2007 Clinical CT-based calculations of dose and positron emitter distributions in proton therapy using the FLUKA Monte Carlo code *Phys. Med. Biol.* **52** 3369

Penfold S N, Schulte R W, Censor Y and Rosenfeld A B 2010 Total variation superiorization schemes in proton computed tomography image reconstruction *Med. Phys.* **37** 5887–95

Podesta M, Persoon L and Verhaegen F 2014 A novel time dependent gamma evaluation function for dynamic 2D and 3D dose distributions *Phys. Med. Biol.* **59** 5973

Rothkamm K and Löbrich M 2003 Evidence for a lack of DNA double-strand break repair in human cells exposed to very low x-ray doses *Proc. of the National Academy of Sciences of the United States of America* vol 100 pp 5057–62

Schulte R *et al* 2004 Nanoparticle-enhanced proton computed tomography: a Monte Carlo simulation study *2004 2nd IEEE Int. Symp. on Biomedical Imaging: Nano to Macro* vol 2 (Arlington, VA: IEEE) pp 1354–6

Schulte R W *et al* 2005 Density resolution of proton computed tomography *Med. Phys.* **32** 1035–46

Schulte R W, Penfold S N, Tafas J T and Schubert K E 2008 A maximum likelihood proton path formalism for application in proton computed tomography *Med. Phys.* **35** 4849–56

Semenenko V A and Stewart R D 2004 A fast Monte Carlo algorithm to simulate the spectrum of DNA damages formed by ionizing radiation **161** 451–7

Semenenko V A and Stewart R D 2006 Fast Monte Carlo simulation of DNA damage formed by electrons and light ions *Phys. Med. Biol.* **51** 1693–706

Shrestha D *et al* 2018 Iterative reconstruction with boundary detection for carbon ion computed tomography *Phys. Med. Biol.* **63** 055002

Stewart R D *et al* 2011 Effects of radiation quality and oxygen on clustered DNA lesions and cell death *Radiat. Res.* **176** 587–602

Stewart R D *et al* 2015 Rapid MCNP simulation of DNA double strand break (DSB) relative biological effectiveness (RBE) for photons, neutrons, and light ions *Phys. Med. Biol.* **60** 8249–74

Stewart R D *et al* 2018 A comparison of mechanism-inspired models for particle relative biological effectiveness (RBE) *Med. Phys.* **45** e925–52

Tessonnier T *et al* 2016 Phase space generation for proton and carbon ion beams for external users' applications at the Heidelberg Ion Therapy Center *Frontiers Oncol.* **5**

Volz L *et al* 2017 Stopping power accuracy and achievable spatial resolution of helium ion imaging using a prototype particle CT detector system *Curr. Dir. Biomed. Eng.* **3** 401–4

Wang G and Jiang M 2004 Ordered-subset simultaneous algebraic reconstruction techniques *J. X-Ray Sci. Technol.* **12** 169–77

Wohlfahrt P *et al* 2017 Dual-energy CT based proton range prediction in head and pelvic tumor patients *Radiother. Oncol.* **125** 526–33

Yang M *et al* 2012 Comprehensive analysis of proton range uncertainties related to patient stopping-power-ratio estimation using the stoichiometric calibration *Phys. Med. Biol.* **57** 4095–115